JAAS

ROYAL SOCIETY OF CHEMISTRY

PAPER

Published on 19 January 2026
Licence and permissions

Check for updates

Cite this: *J. Anal. At. Spectrom.*, 2026, **41**, 1042

Influence of gas flow on elemental analysis using a tandem femtosecond LIBS and LA-ICPMS system

Zhenli Gao,[ab] Wubin Yang, *[ac] Pan Qu,[ac] Shuang Yan,[ac] Chunyi Liu[d] and Richard E. Russo[de]

The integration of LIBS and LA-ICPMS allows for simultaneous determination of a wide range of elements and isotopes. Achieving high-precision quantitative analysis in this dual-technique approach requires establishing the optimal gas environment in the sample chamber. This study evaluated the impact of gas flow on a tandem femtosecond LIBS and LA-ICPMS system. By premixing helium and argon at various ratios, we created gas mixtures with gradient properties. NIST SRM 610 was used as the standard sample to assess the signal intensity and stability of optical emission spectroscopy and mass spectrometry. Our results showed that the LIBS intensity of Li(*I*) 610.35 nm, Li(*I*) 670.77 nm and Ca(*I*) 644.90 nm, along with their relative standard deviation, increased with the proportion of argon in the gas mixture. Conversely, the LA-ICPMS intensity and relative standard deviation of each element decreased with the argon proportion in the carrier gas. LIBS appears to favour an argon ambient gas, while LA-ICPMS prefers helium as the carrier gas. To balance both modules, we tested various helium and argon gas mixtures. A mixed gas composed of 700 ml min^{-1} helium and 400 ml min^{-1} argon was found to be the optimal gas flow for the tandem system, considering signal intensity and relative standard deviation. This study highlights the significant influence of gas flow in optimizing the signal of optical emission spectroscopy and mass spectrometry in a tandem system, enhancing the precision and accuracy of elemental analysis for both modules.

Received 1st September 2025
Accepted 16th January 2026

DOI: 10.1039/d5ja00338e

rsc.li/jaas

1. Introduction

LIBS and LA-ICPMS are widely used for measuring elemental content, providing non-overlapping and complementary information. LIBS can perform a real-time quasi-full elemental analysis of samples in various fields, including coal,[1,2] minerals,[3,4] biological,[5,6] and industrial materials.[7] It is mainly used for sample classification and quantitative determination of major elements including Li, C, N, F, Cl, *etc.* LA-ICPMS is suitable for detecting trace elements with low detection limits[8,9] and facilitates isotopic analyses,[10] which is challenging for LIBS. To combine the advantages of both technologies, the tandem LIBS/LA-ICPMS system has been developed, achieving quantitative analysis,[11–14] discriminant analysis[15–19] and element imaging[20–23] of various materials. This system collects laser plasma and aerosol data simultaneously during a single laser ablation, eliminating positional errors and improving efficiency. By combining the detection advantages of LIBS and LA-ICPMS, it enables the measurement of most elements with ranges from ppt to wt%.

The significance of the gas condition in a tandem system has been highlighted in prior research, with argon benefiting LIBS and helium benefiting LA-ICPMS.[11–23] Latkoczy *et al.*[20] found that the maximum LIBS signal intensity for argon was 2–3 times greater compared to helium or air. Consequently, an argon atmosphere was used in the tandem LIBS/LA-ICPMS system to analyse the elemental distribution in an industrial multi-phase magnesium-based alloy sample. Subedi *et al.*[19] used a tandem LIBS/LA-ICPMS system for analysing printing ink samples, optimizing LIBS acquisition parameters and using argon as the ambient gas for LIBS and carrier gas for LA-ICPMS. Brunnbauer *et al.*[18] analysed epoxy molding compounds using tandem LIBS/LA-ICPMS, selecting helium as the ambient/carrier gas. Since high sensitivity was unrealizable, LIBS was always used to detect main constituents in the wt% range. Dong *et al.*[24] simultaneously determined major elements by LIBS and trace elements by LA-TOF-ICPMS in coal samples, with laser ablation performed in a helium gas flow. Berlo *et al.*[14] conducted analyses of volcanic brines using combined LIBS and ICPMS with pure helium as the gas environment. Nevertheless, these previous studies were limited to either pure helium or pure argon gas flow. Recently, some studies proposed that gas mixtures significantly enhance signal intensity and repeatability

[a]*State Key Laboratory for Deep Earth Processes and Resources, Guangzhou Institute of Geochemistry, Chinese Academy of Sciences, Guangzhou, China. E-mail: yangwubin@gig.ac.cn*

[b]*University of Chinese Academy of Sciences, Beijing, China*

[c]*Guangdong Research Center for Strategic Metals and Green Utilization/Guangdong Provincial Key Laboratory of Mineral Physics and Materials, Guangzhou Institute of Geochemistry, Chinese Academy of Sciences, Guangzhou 510640, China*

[d]*Applied Spectra, 950 Riverside Pkwy Suite 90, West Sacramento, CA 95605, USA*

[e]*Lawrence Berkeley National Laboratory, Berkeley, CA 94720, USA*

compared to pure gas environments in conventional LIBS or LA-ICPMS.[25–27] Yu *et al.* found that the spectral signal intensity and stability of LIBS were higher in gas mixtures than in pure gas environments.[26] Luo *et al.* demonstrated that gas mixtures are more suitable for femtosecond LA-ICPMS analysis.[27] Until now, the impacts of gas mixtures on the signals of the tandem system have not yet been quantitatively evaluated, which are crucial for analytical precision and accuracy.

In this study, a series of helium–argon gas mixtures with varying ratios were systematically tested using a tandem femtosecond LIBS/LA-ICPMS system to evaluate the impacts of gas flow. The quantitative effects of signal intensity, stability, and elemental fractionation in various He–Ar gas mixtures were assessed, as these factors are crucial for the analytical precision of such tandem systems. Subsequently, we propose a significant technical compromise of optimizing the gas flow when using the tandem system of LIBS and LA-ICPMS.

2. Experimental

2.1 Instrumentation

The experimental setup used in this study is illustrated in Fig. 1. NIST 610 silicate glass was analysed in a single sample chamber using a J200 tandem laser ablation. A laser induced breakdown spectroscopy (fsLA-LIBS, Applied Spectra) system equipped with a 343 nm femtosecond pulsed laser, and an iCAP-RQ inductively coupled plasma quadrupole mass spectrometer (ICPMS, Thermo Fisher Scientific) were used. The LIBS system used a Czerny–Turner spectrograph coupled with a high performance ICCD detector (window width of ~100 nm) and a dual grating turret (2400 g mm^{-1} and 1200 g mm^{-1}). The spectrometer was set to a centre wavelength of 645 nm using a 1200 grooves per mm grating, in the wavelength range of 600 to 685 nm, which includes Li(*I*) 610.35 nm, Li(*I*) 670.77 nm and Ca(*I*) 644.90 nm. The gate delay was set to 0.01 μs, gate width was set to 4.0 μs, and intensifier gain was set to 50 (scale from 1 to 100). The laser parameters were an energy density of 5.1 J cm^{-2}, spot size of 50 μm, and repetition rate of 8 Hz, with 200 laser pulses applied at each position. LIBS and LA-ICPMS analyses were performed simultaneously on the same sample spots under identical laser ablation parameters. For ICPMS, NIST 610 silicate glass was ablated for optimizing instrumental parameters. The ICPMS was set to detect a wide range of 59 elements including ^{7}Li, ^{9}Be, ^{11}B, ^{23}Na, ^{25}Mg, ^{27}Al, ^{29}Si, ^{39}K, ^{42}Ca, ^{45}Sc, ^{49}Ti, ^{51}V, ^{52}Cr, ^{55}Mn, ^{59}Co, ^{60}Ni, ^{65}Cu, ^{66}Zn, ^{71}Ga, ^{72}Ge, ^{75}As, ^{85}Rb, ^{88}Sr, ^{89}Y, ^{90}Zr, ^{93}Nb, ^{95}Mo, ^{103}Rh, ^{107}Ag, ^{111}Cd, ^{115}In, ^{118}Sn, ^{121}Sb, ^{133}Cs, ^{137}Ba, ^{139}La, ^{140}Ce, ^{141}Pr, ^{146}Nd, ^{147}Sm, ^{151}Eu, ^{157}Gd, ^{159}Tb, ^{163}Dy, ^{165}Ho, ^{166}Er, ^{169}Tm, ^{173}Yb, ^{175}Lu, ^{179}Hf, ^{181}Ta, ^{182}W, ^{195}Pt, ^{197}Au, ^{205}Tl, ^{208}Pb, ^{209}Bi, ^{232}Th, and ^{238}U. LIBS data were collected using the Applied Spectra Axiom 2.0 software, and ICPMS data were collected using Thermo Fisher Qtegra 2.10.

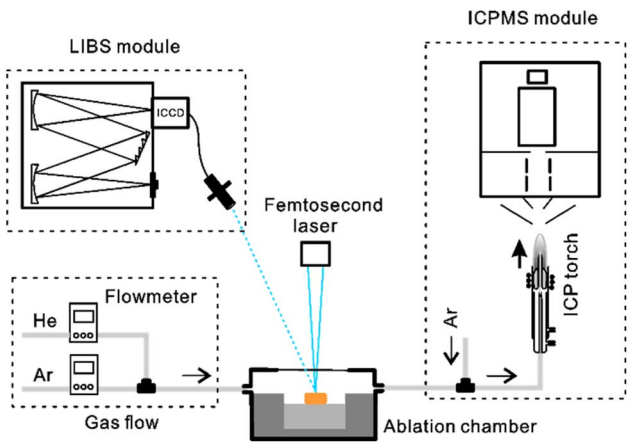

Fig. 1 Experimental setup of the tandem LIBS/LA-ICP-MS system in this study.

2.2 Gas conditions

Helium and argon were selected for the gas mixtures due to their safety, stability, and minimal spectral and polyatomic ion interference in LIBS and LA-ICPMS tests, respectively. A total of 12 different gas mixtures were designed with a 100 ml min^{-1} changing gradient. The composition of each gas mixture, along with their relative molecular weight (M) and ionization energy (E) are listed in Table 1. Note that the type-1 and the type-12 gases are pure He and pure Ar, respectively. Four distinct positions on the sample surface were ablated to evaluate signal stability under each gas condition, with each position subjected to 200 ablation shots. This resulted in the collection of 200 LIBS spectra and 20 seconds of LA-ICPMS signals.

For LIBS data reduction, the average intensity and signal-to-noise ratio (SNR) of each set of 10 spectra were calculated and compared from the 200 collected spectra. The integrated intensity and stability of spectral lines of representative elements in different ambient gases were compared without normalization. For LA-ICPMS data reduction, the signal enhancement factors (SEFs) of each element under different gas conditions relative to pure helium were calculated.[27]

$$\mathrm{SEF} = \frac{\text{Integrated intensity}^{\mathrm{i}}_{\text{type-}n}}{\text{Integrated intensity}^{\mathrm{i}}_{\mathrm{He}}} \quad (1)$$

where Integrated intensity$^{\mathrm{i}}_{\text{type-}n}$ is the integrated signal intensity of element i by LIBS/ICPMS under type-n gas mixture conditions, and Integrated intensity$^{\mathrm{i}}_{\mathrm{He}}$ is the signal intensity of element i by LIBS/ICPMS under pure helium conditions. Additionally, the Ca-normalized fractionation indices (FIs) for all elements and the deviation of their quantitative results from the recommended value were calculated in 12 types of gas environments.[28]

$$\mathrm{FIs} = \frac{\mathrm{Intensity}^{\mathrm{i}}_{\text{last 10 s}} / \mathrm{Intensity}^{\mathrm{Ca}}_{\text{last 10 s}}}{\mathrm{Intensity}^{\mathrm{i}}_{\text{first 10 s}} / \mathrm{Intensity}^{\mathrm{Ca}}_{\text{first 10 s}}} \quad (2)$$

where Intensity$^{\mathrm{i}}_{\text{first 10s}}$ and Intensity$^{\mathrm{i}}_{\text{last 10s}}$ are the average ICPMS signal intensity of element i at the time of the first 10 seconds and last 10 seconds, respectively, and Intensity$^{\mathrm{Ca}}_{\text{first 10s}}$ and Intensity$^{\mathrm{Ca}}_{\text{last 10 s}}$ are the average ICPMS signal intensity of element calcium at the time of early 10 seconds and last 10 seconds, respectively.

2.3 Samples

Silicate glass NIST 610, which is widely used in geochemistry, was used to characterize the emission and mass spectra of the

Table 1 Compositions of 12 types of gas mixtures, and their relative molecular weight (M), and ionization energy (E). Type-1 and type-12 gases are pure helium and argon, respectively

			Gas flow (ml min^{-1})	
Gas type	M	E (kJ mol^{-1})	He	Ar
1	4.0	2372.0	1100	0
2	7.3	2294.6	1000	100
3	10.5	2217.3	900	200
4	13.8	2139.9	800	300
5	17.1	2062.5	700	400
6	20.4	1985.2	600	500
7	23.6	1907.8	500	600
8	26.9	1830.5	400	700
9	30.2	1753.1	300	800
10	33.5	1675.7	200	900
11	36.7	1598.4	100	1000
12	40.0	1521.0	0	1100

tandem system. NIST 610 contains 488 ppm lithium and 8.6 wt% calcium. The peaks of Li(I) 610.35 nm, Li(I) 670.77 nm, and Ca(I) 644.90 nm are easy to measure *via* LIBS, which have high sensitivity and minimal spectral interference. The calibration curve of Li(I) 670.77 nm, established by Fabre *et al.*, indicates that the self-absorption begins at 3000 ppm.[29] And the data of Ca(I) 644.90 nm show an obvious turning point at 500 ppm proposed by Cervantes *et al.*[30] Therefore, lithium and calcium can represent the elements with low concentration not affected by self-absorption and those with high concentration affected by self-absorption, respectively, to characterize changes in LIBS spectra under different gas conditions. This provides a feasible optimization method for detecting more challenging elements (*e.g.*, H, C, N, O, F, molecular information, *etc.*).

A total of 59 elements were detected, with 10 representative elements (including ^{7}Li, ^{42}Ca, ^{60}Ni, ^{66}Zn, ^{88}Sr, ^{90}Zr, ^{139}La, ^{163}Dy, ^{173}Yb, and ^{181}Ta) selected to verify the influence of various gas compositions. These elements include alkali metal elements, transition elements, large ion lithophile elements and high field strength elements, which are of concern in earth and planetary sciences. NIST 612 was used as an external calibration reference, and Ca was used as the internal standard to quantify elemental concentrations in NIST 610 for LA-ICPMS data reduction.[31]

3. Results and discussion

3.1 Selecting strategies of LIBS spectra

A total of 200 spectra were collected per sample position, with 200 laser shots performed under 12 different gas conditions. Fig. 2a and b respectively show the average spectral intensity and signal-to-noise ratio (SNR) of Li(I) 670.77 nm for every 10 shots during a single ablation of NIST 610. Error bars represent the standard deviation (SD) of each set of 10 shots. Gas mixtures with various He–Ar ratios are labelled from type-1 to type-12. Our results show that the stabilities of the average intensity and SNR are relatively good for the first 50 shots, but decrease thereafter. Factors contributing to this decrease include changes in the distance between the ablation site and lens, laser–sample interaction, sampling depth, and optical instability. These changes would affect ablation fluctuations and plasma volume. Given that such fluctuations can be averaged by accumulating laser pulses and spectra,[32] the first 50 laser shots were accumulated for each experiment in this study.

3.2 Signal intensity and repeatability of LIBS within different ambient gases

Based on the discussion above, the average intensity from the first 50 laser shots were selected as the LIBS data. Four sample positions were ablated under 12 different gas conditions. Fig. 3 illustrates the integrated intensity and RSD ($n = 4$) of the first 50 integrals of Li(I) 610.35 nm, Li(I) 670.77 nm, and Ca(I) 644.90 nm in NIST 610 in 12 gas environments. The error bars

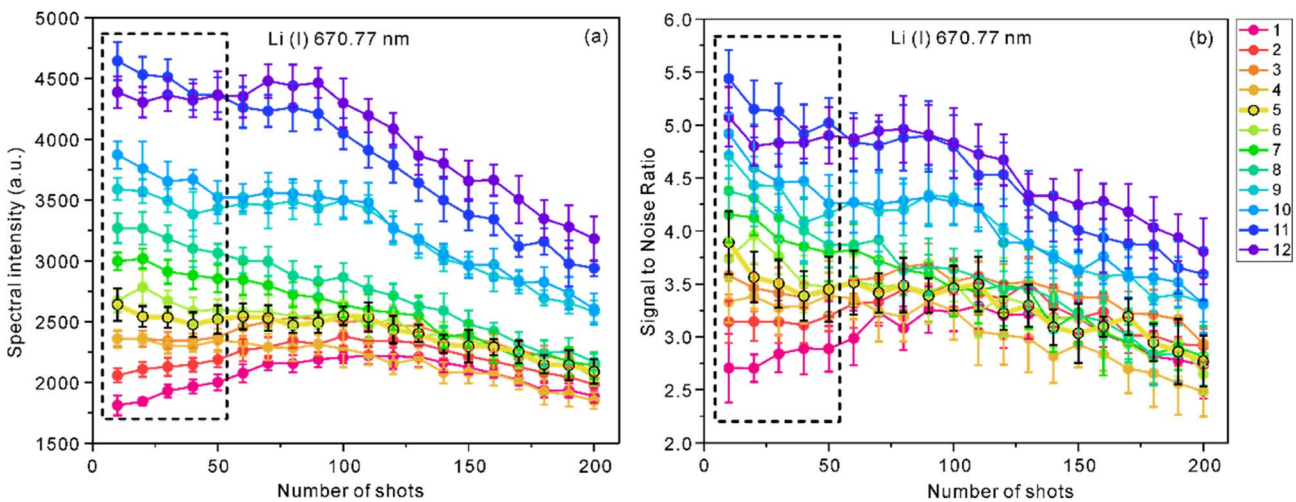

Fig. 2 The average spectral intensity (a) and signal-to-noise ratio (b) of Li(I) 670.77 nm for every 10 shots in a single ablation under 12 gas conditions on NIST 610. 200 spectra were collected at each sample position. Error bars represent the standard deviation (SD, $n = 10$) from every 10 shots. The dashed box highlights the first 50 spectra.

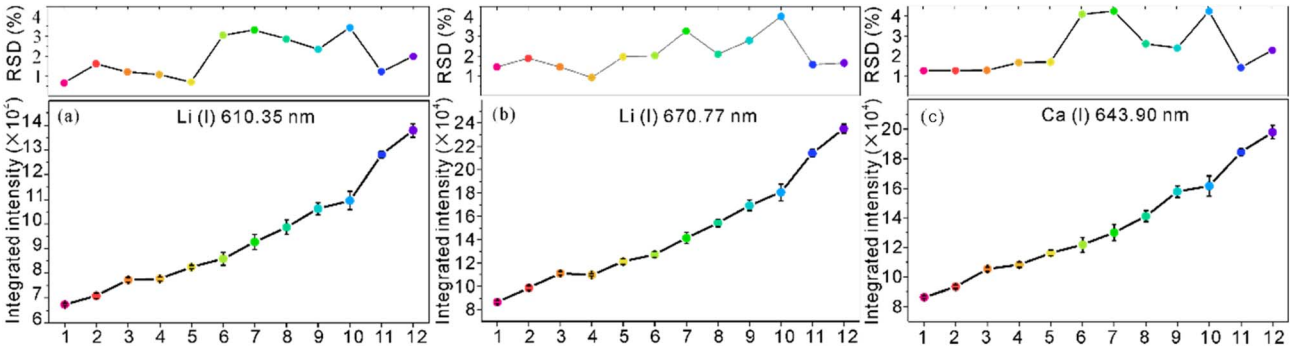

Fig. 3 Integrated intensity and relative standard deviation (RSD, $n = 4$) of Li(*I*) 610.35 nm (a), Li(*I*) 670.77 nm (b), and Ca(*I*) 644.90 nm (c) under 12 gas conditions. Error bars represent the standard deviation (SD, $n = 4$) of integrated intensity from 4 individual sample positions.

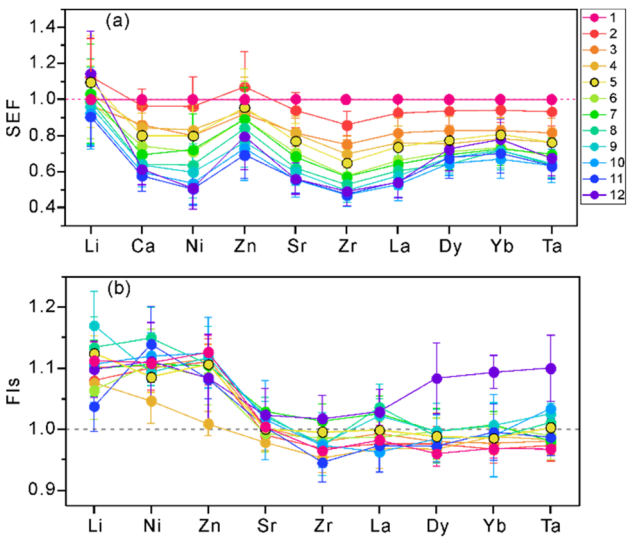

Fig. 4 Signal enhancement factors (SEFs) (a) and fractionation indices (FIs) (b) of representative elements under different gas conditions. SEFs of elements were normalized to the signal intensities of pure He conditions. FIs of elements were normalized to the signal intensities of Ca.

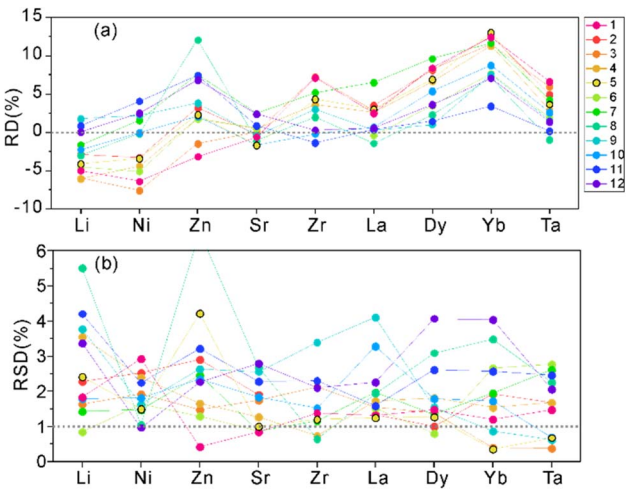

Fig. 5 Relative deviation (RD) (a) and relative standard deviation (RSD) (b) of the representative elements on NIST 610 under 12 gas conditions with 50 μm spot sizes at an energy density of 5.1 J cm^{-2}.

represent the standard deviation (1*s*) of 4 individual analyses. It is evident that the integrated intensity of the peaks for different elements increases significantly from type-1 to type-12 ambient gas. This demonstrates that the increase in the proportion of argon in the mixture significantly enhances the LIBS signal (Fig. 3), consistent with previous studies where signal intensity is proportional to the molecular mass of the ambient gas.[26] Heavier ambient gas influences plasma expansion, making the plasma smaller and denser, and stabilizing its spatial position and shape.[26,33,34] Additionally, the lower the ionization energy of the ambient gas, the greater the tendency of electron generation,[24] increasing electron concentration and enhancing plasma emission intensity. Notably, as the gas changes from type-1 to type-12, the RSD of each condition increases from approximately 1 to 4, indicating a reduction in precision. This can be attributed to the increase in interfacial turbulence caused by the Rayleigh–Taylor instability process,[35] where higher density

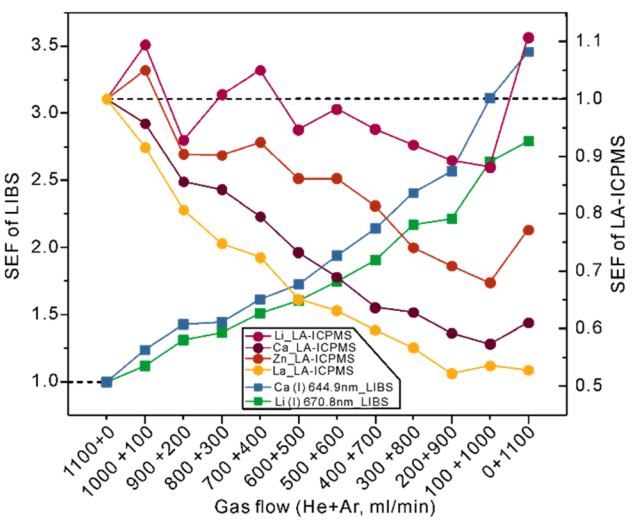

Fig. 6 Comparison of the signal enhancement factor (SEF) for both LIBS and LA-ICP-MS under 12 gas conditions. The signal values under all conditions have been normalized to the type 1 condition (pure He 1100 ml min^{-1}).

contrast between the environment gas and the plasma intensifies their mutual penetration, causing instability in the spectral data.

3.3 Signal intensity and elemental fractionation of LA-ICPMS with different carrier gases

To maintain consistent analysis conditions in the ICP of ^{238}U under different gas conditions, varying flow rates of the makeup gas Ar were introduced *via* a T-piece into the ICPMS. This approach avoided adjusting ICPMS parameters (such as the sample depth or lens position), ensuring that the ^{238}U signal intensity from NIST 610 remained around 3 000 000 counts per second (cps), with a Th/U ratio of approximately 0.65 and a ThO/Th ratio below 0.3%. These conditions satisfied the tuning requirements for general trace element analysis. The SEF of 10 representative elements under 12 gas conditions are shown in Fig. 4a, with all element intensities under different conditions normalized to pure helium (type-1), to verify the effect of different gas conditions on various elements. As the proportion of helium decreased, the SEF of different elements decreased to varying degrees. Given that fs-LA produces ultra-fine particle aerosols, the particle size distribution is less dependent on the carrier gas.[36,37] Our findings indicate that the changes in gas flow affect the ionization efficiency of most elements in ICP. Helium has significant higher thermal conductivity than Ar at *ca.* 5000 K,[38] making it beneficial in improving the ionization efficiency of ICP. A reduction in the proportion of helium in the gas flow leads to decreased ionization efficiency of these elements, resulting in lower signal intensity.

The FIs of elements relative to Ca in NIST 610 for various gas mixtures are shown in Fig. 4b. For more elements, the FIs approach 1 under the type 5 condition. As the amount of argon added to the gas mixtures increases, the FIs of more elements approach 1, indicating reduced fractionation. However, further increases in argon proportion from type 5 lead to increased fractionation, as evidenced by the irregular deviation of elemental fractionation factors from 1 in type 6–12. Using a mixture gas as the carrier gas, a small amount of argon can significantly reduce the signal fractionation of mass spectrometry, but only up to a critical point. This phenomenon may be linked to the properties of the carrier gas, such as relative molecular mass, ionization potential, and thermal conductivity, while the properties of the mixture lie between those of pure helium and argon. The interplay of these properties affects the ICP, leading to an element fractionation decrease with the argon proportion of the carrier gas.

3.4 Combining LIBS and LA-ICPMS for elemental analysis

When the helium and argon mixture is used as the ambient/carrier gas of the tandem femtosecond system, a slight increase in argon can reduce the fractionation in mass spectrometry analysis, and also reduce the sensitivity of most elements. Therefore, we calculated the relative deviation (RD) and relative standard deviation (RSD) of the concentrations of each element in NIST 610 at various gas mixtures to evaluate the quality of data. NIST 612 was used as the external standard, while Ca was used as the internal standard. Fig. 5a shows the RD of the determined concentration ($n = 4$) of NIST 610 relative to the reference value under 12 gas conditions, representing the accuracy of the quantitative results. For the 12 gas mixtures, the RD of most elements is within 10%. As the proportion of argon in the gas increases, the RD of the most elements slowly approaches 0, indicating improved data accuracy. Fig. 5b shows the RSD of the determined concentration ($n = 4$) of NIST 610 under 12 gas conditions, representing the precision of the quantitative results. The RSD of quantitative results for more elements in type 5 is close to 1, which is close to the data quality obtained under pure helium conditions.

Tandem LIBS and LA-ICPMS enables the detection of a broad spectrum of elements and isotopes. This combination leverages the benefits of two techniques, creating a robust and versatile analytical tool. As shown in Fig. 6, the SEF of LIBS increases with the increase in the proportion of argon in the gas mixtures, while the SEF of LA-ICPMS shows an overall decreasing trend. A compromise can be achieved in the tandem system by using the gas mixtures, which can enhance the LIBS signal quality without affecting the LA-ICPMS data quality.

4. Conclusion

This study investigated the effects of pre-mixed argon and helium in various proportions as the ambient/carrier gas on the spectral and mass spectrometric data for optimizing the analytical conditions of the combined analysis. The results of this study indicate that when using a type-5 gas mixture as the ambient/carrier gas for the tandem femtosecond LIBS and LA-ICPMS system analysis, it yields higher intensity and stability of the spectral signal compared to using pure gas or other proportionally mixed gas. This study, for the first time, demonstrates that using a mixed gas as the ambient/carrier gas for the femtosecond tandem LIBS and LA-ICPMS system enhances its quantitative analysis of various samples, resulting in more accurate and stable spectral and mass spectrometric data. The relationship between gas properties and the LIBS and LA-ICPMS signals was examined. However, the mechanism by which these gas properties affect plasma parameters and aerosol states excited by a femtosecond laser is not fully understood and requires further investigation. Additionally, the influence of gas composition on ionic or molecular lines in LIBS, and the effects of other optimization parameters (sample depth, lens position, *etc.*) on the elemental sensitivity in LA-ICPMS would be investigated in a future study.

Conflicts of interest

The authors declare no competing interests.

Data availability

All data supporting the findings of this study are available within the paper and its supplementary information (SI). Supplementary information is available. See DOI: https://doi.org/10.1039/d5ja00338e.

Acknowledgements

We are grateful to the science editor for efficient handling, and to the four anonymous reviewers for their insightful comments, which immensely improved the manuscript. This work was financially supported by the Science and Technology Planning Project of Guangdong Province (2024B0303390002), the National Key Research and Development Program of China (2021YFC2901705), and the National Natural Science Foundation of China (42302092).

References

1 S. Sheta, M. S. Afgan, Z. Hou, S.-C. Yao, L. Zhang, Z. Li and Z. Wang, *J. Anal. At. Spectrom.*, 2019, **34**, 1047–1082.
2 K. Liu, C. He, C. Zhu, J. Chen, K. Zhan and X. Li, *TrAC, Trends Anal. Chem.*, 2021, **143**, 116357.
3 T. Chen, T. Zhang and H. Li, *TrAC, Trends Anal. Chem.*, 2020, **133**, 116113.
4 R. S. Harmon and G. S. Senesi, *Appl. Geochem.*, 2021, **128**, 104929.
5 Q. Wang, W. Xiangli, G. Teng, X. Cui and K. Wei, *Appl. Spectrosc. Rev.*, 2020, **56**, 221–241.
6 S. J. Rehse, H. Salimnia and A. W. Miziolek, *J. Med. Eng. Technol.*, 2012, **36**, 77–89.
7 S. Legnaioli, B. Campanella, F. Poggialini, S. Pagnotta, M. A. Harith, Z. A. Abdel-Salam and V. Palleschi, *Anal. Methods*, 2020, **12**, 1014–1029.
8 D. E. Jacob, *Geostand. Geoanal. Res.*, 2006, **30**, 221–235.
9 T. Hirata and Y. Kon, *Anal. Sci.*, 2008, **24**, 345–352.
10 A. R. C. Kylander-Clark, *Rev. Mineral. Geochem.*, 2017, **83**, 183–198.
11 M. Dong, D. Oropeza, J. Chirinos, J. J. González, J. Lu, X. Mao and R. E. Russo, *Spectrochim. Acta, Part B*, 2015, **109**, 44–50.
12 M. Bonta and A. Limbeck, *J. Anal. At. Spectrom.*, 2018, **33**, 1631–1637.
13 Y. Lee and H. Kim, *Anal. Sci. Technol.*, 2019, **32**, 121–130.
14 K. Berlo, V. van Hinsberg, R. Lauzeral, F. Zwillich and J. Gonzalez, *Chem. Geol.*, 2022, **603**, 120910.
15 Y. Lee, S.-H. Nam, K.-S. Ham, J. Gonzalez, D. Oropeza, D. Quarles, J. Yoo and R. E. Russo, *Spectrochim. Acta, Part B*, 2016, **118**, 102–111.
16 M. Dong, L. Wei, J. J. Gonzalez, D. Oropeza, J. Chirinos, X. Mao, J. Lu and R. E. Russo, *Anal. Chem.*, 2020, **92**, 7003–7010.
17 L. Brunnbauer, M. Mayr, S. Larisegger, M. Nelhiebel, L. Pagnin, R. Wiesinger, M. Schreiner and A. Limbeck, *Sci. Rep.*, 2020, **10**, 12513.
18 L. Brunnbauer, V. Zeller, Z. Gajarska, S. Larisegger, S. Schwab, H. Lohninger and A. Limbeck, *Spectrochim. Acta, Part B*, 2023, **207**, 106739.
19 K. Subedi, T. Trejos and J. Almirall, *Spectrochim. Acta, Part B*, 2015, **103–104**, 76–83.
20 C. Latkoczy and T. Ghislain, *J. Anal. At. Spectrom.*, 2006, **21**, 1152–1160.
21 J. R. Chirinos, D. D. Oropeza, J. J. Gonzalez, H. Hou, M. Morey, V. Zorba and R. E. Russo, *J. Anal. At. Spectrom.*, 2014, **29**, 1292–1298.
22 B. T. Manard, C. Derrick Quarles, E. M. Wylie and N. Xu, *J. Anal. At. Spectrom.*, 2017, **32**, 1680–1687.
23 O. Syta, B. Wagner, E. Bulska, D. Zielinska, G. Z. Zukowska, J. Gonzalez and R. Russo, *Talanta*, 2018, **179**, 784–791.
24 M. Dong, X. Mao, J. J. Gonzalez, J. Lu and R. E. Russo, *J. Anal. At. Spectrom.*, 2012, **27**, 2066–2075.
25 D. Gunther and C. A. Heinrich, *J. Anal. At. Spectrom.*, 1999, **14**, 1363–1368.
26 J. Yu, Z. Hou, Y. Ma, T. Li, Y. Fu, Y. Wang, Z. Li and Z. Wang, *Spectrochim. Acta, Part B*, 2020, **174**, 105992.
27 T. Luo, Q. Ni, Z. Hu, W. Zhang, Q. Shi, D. Günther, Y. Liu, K. Zong and S. Hu, *J. Anal. At. Spectrom.*, 2017, **32**, 2217–2225.
28 B. J. Fryer, S. E. Jackson and H. P. Longerich, *Can. Mineral.*, 1995, **33**, 303–312.
29 C. Fabre, M.-C. Boiron, J. Dubessy, A. Chabiron, B. Charoy and T. M. Crespo, *Geochim. Cosmochim. Acta*, 2002, **66**, 1401–1407.
30 C. Cervantes, B. S. Marangoni, G. Nicolodelli, G. S. Senesi, P. R. Villas-Boas, C. S. Silva, A. R. A. Nogueira, V. M. Benites and D. M. B. P. Milori, *Minerals*, 2024, **14**(11), 1109.
31 N. Miliszkiewicz, S. Walas and A. Tobiasz, *J. Anal. At. Spectrom.*, 2015, **30**, 327–338.
32 R. Wisbrun, I. Schechter, R. Niessner, H. Schroder and K. L. Kompa, *J. Appl. Phys.*, 2002, **66**, 2964–2975.
33 S.-B. Wen, X. Mao, R. Greif and R. E. Russo, *Anal. Chem.*, 2007, **101**, 023115.
34 A. Bogaerts, Z. Chen and D. Bleiner, *J. Anal. At. Spectrom.*, 2006, **21**, 384–395.
35 V. Y. Baranov, O. N. Derkach, V. G. Grishina, M. F. Kanevskii and A. Y. Sebrant, *Phys. Rev. E: Stat. Phys., Plasmas, Fluids, Relat. Interdiscip. Top.*, 1993, **48**, 1324–1330.
36 C. C. Garcia, M. Wälle, H. Lindner, J. Koch, K. Niemax and D. Günther, *Spectrochim. Acta, Part B*, 2008, **63**, 271–276.
37 J. Koch, A. von Bohlen, R. Hergenröder and K. Niemax, *J. Anal. At. Spectrom.*, 2004, **19**, 267–272.
38 H. Niu and R. S. Houk, *Spectrochim. Acta, Part B*, 1996, **51**(8), 779–815.